AIChE WILEY InterScience DISCOVER SOMETHING GREAT

Instability of Bounded Gas-Particle Fluidized Beds

Xue Liu and Benjamin J. Glasser
Dept. of Chemical and Biochemical Engineering, Rutgers University, Piscataway, NJ, 08854

Maureen A. Howley
Dept. of Chemical Engineering, New Jersey Institute of Technology, Newark, NJ, 07102

DOI 10.1002/aic.11134
Published online March 2, 2007 in Wiley InterScience (www.interscience.wiley.com).

Steady flows of gas and particles in unbounded-fluidized beds have been shown to lose stability to localized voidage disturbances. An insight is provided into the linear stability of bounded gas-particle flows using a kinetic theory approach. The stability analysis is carried out for two illustrative sets corresponding to fluidized systems having walls acting as sinks *and* sources *of fluctuation energy. Instabilities are characterized by computing leading eigenvalue profiles and dominant eigenfunction contour maps. Results show two types of dominant instability patterns (symmetric and antisymmetric) for flow in a vertical duct, both of which propagate through the bed in the form of traveling waves at speeds comparable to that of the solid phase. Moreover, model predictions show that increasing solids fraction and decreasing particle inelasticity will suppress the wavy disturbance. The physical mechanism of instability formation is further investigated using a term-by-term method of analysis. Results show that instability modes can be suppressed if solid phase inertia or inelastic particle collisions are eliminated from the momentum and pseudo-thermal energy balance equations. Finally, the symmetric instabilities were shown to develop into bubble-like structures while the antisymmetric instabilities develop into streamer-like structures.* © 2007 American Institute of Chemical Engineers *AIChE J,* 53: 811–824, 2007

Keywords: gas-fluidized beds, linear-stability analysis, kinetic theory, coefficient of restitution, solids fraction, inertial forces

Introduction

Gas-fluidized beds are used extensively in chemical, petrochemical and pharmaceutical industries. Although some gas-particle-fluidized beds can present a smooth appearance, expanding progressively at flow rates well beyond the minimum fluidization velocity, most gas-particle systems are unstable to low-amplitude disturbances and develop nonuniform-particle distributions in the form of voidage waves. Such nonuniformities can become amplified in the bed to form fully developed bubbles (in dense fluidized beds),[1] clusters and streamers (in dilute fluidized beds)[2–4] and slugs (in narrow fluidized beds).[1] Although the presence of voidage or density waves are known to dramatically impact process safety and economics (by affecting heat and mass transfer rates), the underlying physical mechanisms responsible for unstable-flow behavior are still not fully understood.

Using continuum mechanics, volume- or ensemble-averaged equations of mass and motion have been postulated to describe the flow of the fluid and particle phases in fluidized beds.[5] It is common to derive the constitutive relations for the solid phase momentum equation from the kinetic theory

Correspondence concerning this article should be addressed to B. J. Glasser at bglasser@rutgers.edu.

of dense gases.[6–9] The main difference between molecular gases and granular particles is that energy is lost due to collisions between particles, while this is not true for molecular-gas collisions.

For unbounded gas-particle flows, the simplest solution to the governing equations of motion represents the steady state of uniform fluidization. In order to predict the growth of disturbances from the steady base state, conventional methods of hydrodynamic stability analysis have been applied.[10–17] The earliest stability analysis from the work of Jackson[14] predicted that uniform-fluidized beds are inherently unstable, and that such instabilities are in the form of plane waves, which propagate vertically upward through the bed. Although linear theory can account for the existence of traveling waves in gas-fluidized beds, it can only capture phenomena occurring in close proximity to the marginal stability point. Therefore, it is not capable of predicting the ultimate fate of the instability. In order to better understand the origin of the bubbly-flow regime, the nonlinear terms in the equations of motion have been taken into account in one-dimensional (1-D) fluidized beds.[18–21] Results of nonlinear analyses have shown that low-amplitude disturbances can become amplified in the bed to form fully-developed 1-D traveling waves.[21]

Bifurcation theory has also been used to investigate the behavior of traveling waveforms in fluidized beds.[22–26] Using bifurcation analysis and a numerical continuation approach, Glasser et al.[22,25] demonstrated that 1-D traveling wave solutions bifurcating from the uniform base state are unstable in the transverse direction, and that this can lead to the formation of bubble-like structures. It was later established by these same authors that bubbles and clusters belong to the same family of nonuniform traveling wave solutions.[26]

Anderson and Jackson were the first to attempt to experimentally measure the properties of growing waves.[27] More systematic studies were, subsequently, carried out by El-Kaissy and Homsy.[28] These researchers observed from a uniform fluidization state the exponential growth of 1-D wave trains in the vertical direction at distances well above the distributor plate. Moreover, secondary instabilities generated from the breakdown of the primary wave train were also observed when the amplitude of the primary wave was sufficiently large. The fact that the 1-D vertical wave train is unstable to transverse structures under certain conditions was conjectured to reveal the origin of bubbling behavior.

It is important to note that in the literature, theoretical studies involving stability analyses of gas-fluidized beds have been restricted to unbounded systems, where the steady-state solution describes a spatially uniform fluidization state. In bounded gas-particle flows, however, particles will normally segregate.[29–31] Clearly then, the flow characteristics of the base state, for example., pressure gradient and interstitial gas and particle velocity profiles, will depend on a nonuniform-particle distribution. A number of theoretical studies have been conducted in the past 20 years to analyze the steady-state solutions describing fully developed gas-particle flows in a vertical tube using kinetic theory to describe the averaged quantities in the solid phase.[32–35] These continuum models predict a variety of flow behaviors occurring in risers and standpipes, including packed beds, uniformly-fluidized beds, choking, flooding and the existence of multiple steady-states. However, it is not clear whether these nonuniform steady-state flow profiles can be observed in real fluidized-bed operations. Thus, a further investigation of the hydrodynamic stability of these nonuniform systems is required.

A long term goal of this research is to perform a full bifurcation and stability analysis of gas-fluidized beds. To that end, a linear stability analysis of the steady-state solution is first carried out to examine whether or not the base state is stable, and if unstable, what nonuniform instability structures can arise. Although a direct integration of the volume-averaged equations of motion can predict time-dependent flow behavior in the bed, this approach cannot capture important stability features or determine the nature of instabilities generated from the base state. It is this behavior that is of particular interest for developing a better understanding of gas-particle flows.

While the ultimate behavior of the bed is known to be governed by nonlinear dynamics, an understanding of the effect of the linear terms (on instability behavior) will most likely offer insight into the effect of the nonlinear terms for both short term and long term durations. In a linear stability study conducted by Wang et al.[36] involving fully developed rapid flow of a granular material in a channel, it was shown that when the base state was unstable, the fastest growing modes are traveling waves propagating in the vertical direction. Wang et al.[37] later studied the transient development of linear instability waves for granular flows in a channel. For the short term, they found the temporal development of granular flow is dominated by the linear instability, and, in some cases, the linear terms continue to dominate flow development for the long term.

In this work, we first seek steady-state solutions to the governing equations of continuity and motion describing a gas-fluidized bed, which is bounded by walls, using closures adopted from kinetic theory. The stability of the base state is, subsequently, examined using classical methods of linear stability theory to examine the nature of instabilities, the structure of unstable waveforms (for example, bubbles, streamers and slugs), and the effect of various physical parameters on instability formation. Results provide an explanation of experimentally observed flow features, which are associated with fluctuation behavior in gas-particle fluidized beds, and test the feasibility of using a kinetic theory approach for providing closures.

Governing Equations and Numerical Method

A continuum model is used to simulate gas-particle flow in a channel, where gas flows vertically upward through a bed of packed particles until the gas velocity is sufficient to suspend the particles in the fluid phase. This occurs at some minimum fluidization velocity when the drag force overcomes the gravitational weight of the particles corrected for buoyancy.

The continuity and momentum balance equations for the gas and solids phases are used in this study. They take the following form from the work of Anderson and Jackson[10]

$$\frac{\partial \phi}{\partial t} + \nabla \cdot (\phi \underline{v}) = 0 \tag{1}$$

$$\frac{\partial(1-\phi)}{\partial t}+\nabla\cdot[(1-\phi)\underline{u}]=0 \tag{2}$$

$$\rho_s\phi\left[\frac{\partial \underline{v}}{\partial t}+\underline{v}\cdot\nabla\underline{v}\right]=-\nabla\cdot\underline{\underline{\sigma_s}}-\phi\nabla\cdot\underline{\underline{\sigma_f}}+\underline{f}+\phi\rho_s\underline{g} \tag{3}$$

$$\rho_f(1-\phi)\left[\frac{\partial \underline{u}}{\partial t}+\underline{u}\cdot\nabla\underline{u}\right]=-(1-\phi)\nabla\cdot\underline{\underline{\sigma_f}}-\underline{f}+(1-\phi)\rho_f\underline{g} \tag{4}$$

Here, ϕ denotes the locally averaged-volume fraction of particles; $\underline{v}$ and $\underline{u}$ denote the locally averaged velocities of the solid and gas phases, respectively; ρ_s and ρ_f are the respective densities of the solid and gas phases; $\underline{g}$ is the gravity force vector pointing in the negative vertical direction ($-x$); $\underline{f}$ is the force per unit volume exerted by the gas on the particles; $\underline{\underline{\sigma_s}}$ and $\underline{\underline{\sigma_f}}$ are the effective stress tensors for the solid and gas phases, respectively. Since the density of the gas phase is much smaller than the solid phase, the contribution of the force of virtual mass is neglected in this study. In kinetic theory, the solid-phase stress depends on the granular temperature. Therefore, an equation representing the balance of pseudo-thermal energy (PTE) is required[4]

$$\frac{\partial(\frac{3}{2}\rho_s\phi T)}{\partial t}+\nabla\cdot\left(\frac{3}{2}\rho_s\phi T\underline{v}\right)=-\nabla\cdot\underline{q}-(\underline{\underline{\sigma_s}}:\nabla\underline{v})-J_{coll}-J_{vis} \tag{5}$$

where T denotes the granular temperature, which is proportional to the mean square of particle-fluctuation velocity. The two terms on the lefthand side represent the rate of accumulation and the rate of transport of PTE. On the righthand side, the divergence of the granular energy flux $\nabla\cdot\underline{q}$, represents the diffusive transport of PTE, and $(\underline{\underline{\sigma_s}}:\nabla\underline{v})$ represents the rate of production of PTE by particle-particle shear. J_{coll} denotes the rate of dissipation of PTE through inelastic collisions, and J_{vis} denotes viscous damping and the production of PTE by gas-particle slip. The constitutive relations for, $\underline{\underline{\sigma_s}}$, $\underline{\underline{\sigma_f}}$, $\underline{f}$, $\underline{q}$, J_{coll} and J_{vis} are those adopted by Liu and Glasser.[35] Boundary conditions for particulate and gas-particle flows have been investigated in a number of articles.[38–41] The boundary conditions used in this work for the gas phase and solid-phase momentum balance and pseudo-thermal energy balance are discussed by Liu and Glasser.[35]

In the absence of walls, the equations of motion have a solution representing a uniformly fluidized bed, where (upon average), particles are suspended in the fluidization state and particle distribution and bed composition is homogeneous throughout. With walls, the base state of the gas-particle flow is not uniform. Instead, segregation of particles can be observed. For steady, fully-developed flows all fluid dynamics variables are functions of the lateral (y) direction, and the two-phase continuity Eqs. 1 and 2 are identically satisfied. Using ρ_s, v_t (particle-terminal velocity), Δ (half of the bed width), and Δ/v_t, μ_g (pure-gas viscosity) as the characteristic density, velocity, length, time and gas-phase viscosity, respectively, the 2-D momentum and pseudo-thermal energy Eqs. 3, 4 and 5, and boundary conditions can be cast in the dimensionless form[35]. The steady-state solutions are obtained using two numerical schemes to verify correctness: an orthogonal collocation approach[42] and a second-order finite difference method. In this work, the results are presented in dimensionless form

$$u_x^*=\frac{u_x}{v_t}\qquad v_x^*=\frac{v_x}{v_t}\qquad T^*=\frac{T}{v_t^2}\qquad D=\frac{\Delta}{d}$$
$$E=\frac{\rho_g}{\rho_s}\qquad x^*=\frac{x}{\Delta}\qquad y^*=\frac{y}{\Delta}$$

The linear stability of the base state is examined by imposing a perturbation on the steady-state solution in the form of a localized periodic disturbance. The governing equations and boundary conditions are then expanded in ascending powers of the perturbations through a Taylor series expansion of the nonlinear terms. Since the disturbances are assumed to be both small and smoothly varying in space and time, their derivatives are also small. Therefore, all terms of degree greater than one in the perturbations are neglected. Perturbations are assumed to take the form of a plane wave disturbance. For example, the steady-state solution for volume fraction (ϕ_0) is augmented with a perturbation in solids fraction, ϕ_1, in the form of a plane wave disturbance

$$\phi_1=\hat{\phi}_1\exp(st^*)\exp(\underline{K}\cdot\underline{X}^*) \tag{6}$$

$\hat{\phi}_1$ is the complex amplitude, which is a function of the lateral space. In this expression, $\underline{X}^*$ represents the dimensionless position vector $\underline{X}^*=(x^*, y^*, z^*)$, and the dimensionless wave-number vector of the plane wave disturbance is $\underline{K}=(k_x, k_y, k_z)$. For a 2-D disturbance in a bounded gas-particle fluidized bed, $\exp(\underline{K}\cdot\underline{X}^*)$ can be written as $\exp(k_x x^*)$, where k_x represents the dimensionless wave number in the vertical direction, and the disturbance in the lateral direction comes from $\hat{\phi}_1$. In general, the eigenvalue s is a complex number which may be written as $s=\xi-i\omega$. The imaginary part ω then determines v_p^*, the dimensionless velocity of propagation of the waves, according to $v_p^*=\omega/k_x$, while the real part ξ, or growth rate, determines the rate of growth, or decay of the waves with time depending on its signage. That is, if ξ is positive, the disturbance grows in time, and the base state is unstable, and if ξ is negative, the disturbance decays and the base state is stable. The growth distance, Δx^*, can be defined by $\Delta x^*=\omega/(\xi\, k_x)$.

Linearization results in a set of ordinary differential equations (ODE's) written in terms of perturbation variables.[43] Since no boundary conditions exist for ϕ and P_f, a staggered grid spectral collocation scheme is employed. The continuity equations are collocated at points lying between the collocation points for the momentum and energy equations. This reduces the number of unknowns by two. The ODE's are then discretized leading to a matrix eigenvalue problem, which takes the form

$$AZ=sBZ \tag{7}$$

where Z is an array representing the unknowns. Since boundary conditions do not contain the eigenvalue s, and the coefficients of s in the gas-phase continuity can be eliminated using those in the solid-phase continuity equations, B is a singular matrix. This singularity can be removed by row and column operations. The resulting eigenvalue problem is solved using Matlab 6.5.[43]

Table 1. Basic simulation parameters

d	Particle diameter	500 μm
μ_g	Viscosity of gas	0.00004 kg/(ms)
ϕ_{max}	Maximum solid volume fraction	0.65
ρ_g	Gas density	3 kg/m^3
ρ_s	Solid density	2000 kg/m^3
g	Gravitational acceleration	9.81 N/kg
$2\Delta/d$	Ratio of bed width to particle diameter	60
φ'	Specularity coefficient	0.6

The accuracy of the numerical scheme is ascertained by increasing the number of collocation points until the leading eigenvalue converges to a value independent of the variation in number of collocation points. Computational results show that the larger the value of k_x, the larger the number of collocation points required for convergence. To ensure accuracy, our simulation code was favorably compared with published results from the literature.[44] A comparison with experimental work was also carried out by investigating the stability of unbounded-fluidized beds with a uniform steady-state, using Eqs. 1–5. We found the dominant instability from the uniform state is a vertical traveling wave, which propagates faster than the superficial gas velocity.[43] This is in agreement with experimental measurements.[27,28]

The physical parameters used in this article are shown in Table 1. In this work we mainly focus on the effect of mean-solids fraction, particle-particle restitution coefficient, and particle-wall restitution coefficient, while holding other parameters constant. We have also investigated the effect of changing the specularity coefficient, and found that the steady-state solutions and instability modes are insensitive to this parameter. We have also doubled the density ratio, and ratio of bed width to particle diameter (relative to the values in Table 1), and observed no qualitative difference in the instability patterns.

Results and Discussion

This work focuses on gaining a better understanding of the effect of walls on unstable-flow behavior in gas-particle systems, having spatially nonuniform steady-states. In our model, two parameters are used to describe the wall properties. One is the coefficient of particle-wall restitution (e_w), and the other is the specularity coefficient. We start by investigating the effect of the coefficient of particle-wall restitution, since it is known that inelasticity has a significant effect on system instability.[37] Wang et al.[36,45] reported that the presence of walls in granular flow within a channel could serve as either a *source* or a *sink* of fluctuation energy depending on the value of e_w and e_p. The coefficient of particle-particle restitution (e_p) quantifies the inelasticity of particle-particle collisions. e_p and e_w ranges from zero (perfectly ineleastic) to one (perfectly elastic). In particular, for flow conditions where $e_w < e_p$, the wall serves as a *sink* of fluctuation energy, that is, the gradient in granular temperature is negative toward the walls. For conditions where $e_p < e_w$, the wall serves as a *source* of fluctuation energy, that is, there exists a flux of pseudo-thermal energy from the walls to the particle assembly.[36]

Base-state profiles of solids-volume fraction (ϕ), (dimensionless) granular temperature (T^*), and (dimensionless) gas and particle velocities (u^* and v^*) for the source and sink-wall conditions are shown in Figures 1 and 2, respectively, for cocurrent upflow. To better investigate the effect of wall properties, the value of e_p is held constant at 0.96, and the

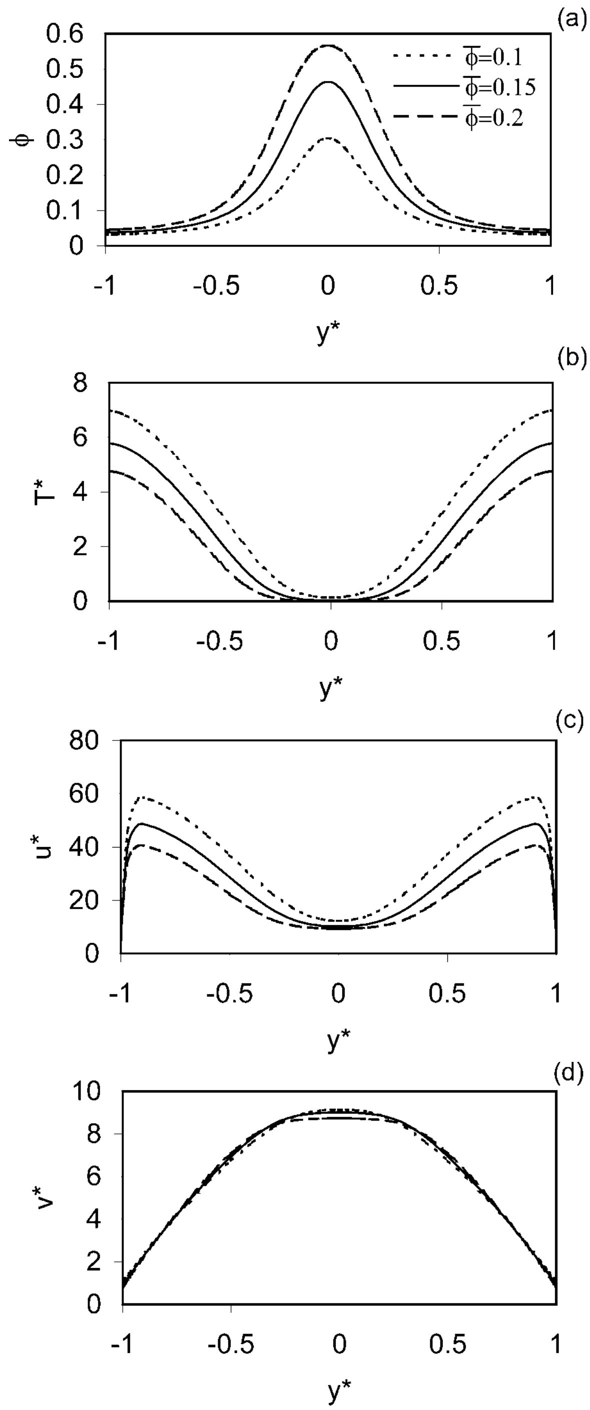

Figure 1. Steady-state profiles for the source-wall condition, e_p = 0.96, e_w = 0.98.

(a) solids fraction, (b) granular temperature, (c) gas velocity, and (d) solids velocity.

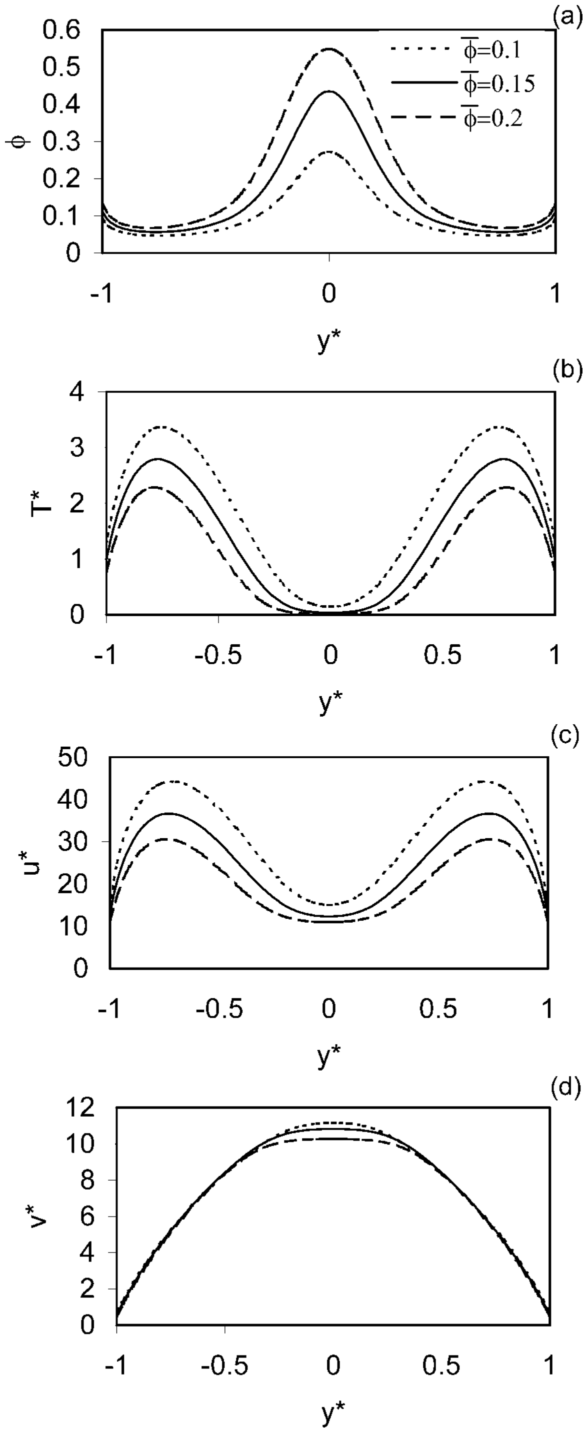

Figure 2. Steady-state profiles for the sink-wall condition, e_p = 0.96, e_w = 0.6.

(a) solids fraction, (b) granular temperature, (c) gas velocity, and (d) solids velocity.

value of e_w is varied from 0.6 for the sink-wall condition to 0.98 for the source-wall condition. When the wall is a *source* of fluctuation energy, we see in Figure 1a that ϕ monotonically decreases when moving away from the center toward the walls, and that this corresponds to an increase in granular temperature T^* (see Figure 1b). An inverse relationship between ϕ and T^* is predicted by Eq. 3, which requires the solid concentration be small in regions where the granular temperature is large, and vice versa. If the average solids fraction is high enough, a plug flow can be observed where $\phi = \phi_{max}$ (maximum solids fraction $\phi_{max} = 0.65$) at the center. Variations in u^* and v^*, for the source-wall condition are shown in Figure 1c and d, respectively. In Figure 1d, v^* reaches a maximum value in the center, and monotonously decreases toward the wall. In Figure 1c, u^* is shown to initially increase as one moves away from center, and then passes through a maximum value corresponding to high-values in the granular-temperature profile. As the wall is approached, u^* is shown to rapidly decrease. The relationship between the granular temperature and the superficial-gas velocity predicted, using this model has been observed in experiments.[46,47]

In Figure 2a we see that the solids-volume fraction profile for the wall *sink* condition is very similar to the source wall case in Figure 1a, except in the region very near the wall where a slight increase in ϕ is observed. This can be explained by the fact that the granular temperature decreases close to the walls in this case. T^* is shown to increase away from the center, passes through a maximum, and finally decreases rapidly near the walls. Profiles of v^* and u^* are very similar to the source-wall case, except that the maximum value of u^* is more pronounced under the source condition (Figure 1c) than the sink condition (Figure 2c), due to higher values of T^* near the walls (see Figure 1b vs. Figure 2b).

We have shown that profiles of solids-volume fraction are very similar for both sink and source-wall cases in Figures 1a and 2a with the exception of the region adjacent to the walls. Hence, e_w plays only a minor role within the range of 0.6 to 0.98 as shown. However, the similarity in profile is strongly dependent on the value of e_p. We find for e_p very close to 1, profiles for ϕ and T^* differ qualitatively and quantitatively, as one approaches the wall (not shown). For the sink-wall condition ($e_w = 0.6$), and a value of e_p of 0.99, the increase in ϕ near the walls becomes so pronounced that the solids fraction at the walls is almost as large as that at the center. This is unlike the source-wall case ($e_w = 0.99$, $e_p = 0.99$), where particle concentration monotonically decreases from the center to the walls. Hence, particle concentration at the center is much higher under the source-wall condition than the sink-wall condition.

Computational results from previous work have led researchers to propose that for $e_p \approx 1$, particles are sequestered near the walls leaving the core of the reactor occupied by a dilute region with high-gas flow rate.[32–34] This "Core-Annular" flow structure in gas-particle fluidized beds has been discussed in many articles and widely reported in the experimental literature.[29,48–50] It is clear that for a fixed value of e_w the flow structure may transition from a "Core-Annular" structure to segregation of particles to the center for values of $e_p < 1$, and that this transition is very sensitive to e_p when its value is close to 1. With a further decrease in e_p, it was shown that flow profiles are no longer sensitive to e_p.[35] If both e_p and e_w are assumed equal to 1, a solution with a uniform solids fraction will be obtained from the simulations.

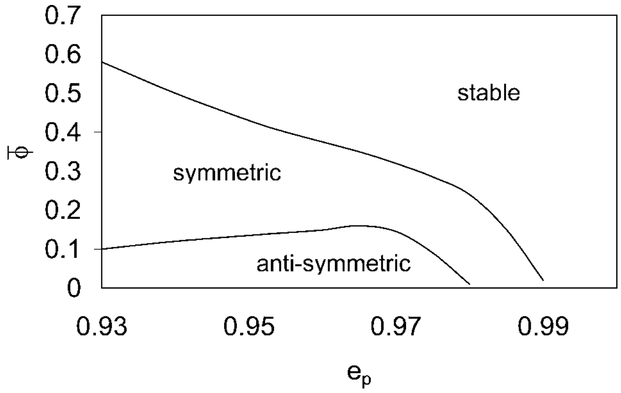

Figure 3. Contours of the instability patterns of the dominant eigenvalues in the e_p – $\bar{\phi}$ plane.

When e_w is small, the walls act as an energy sink for fluctuation energy. Under these conditions, the stability structure map in the $\bar{\phi} - e_p$ plane (average solids-volume fraction — coefficient of restitution) is shown in Figure 3. In this work, the eigenvalue s having maximum positive growth rate, ξ, at a vertical wave number k_x is referred to as the *leading* eigenvalue, and s having maximum ξ for all k_x, is referred as the *dominant* eigenvalue. Within the physical parameter space, the stability analysis shows the dominant mode in the $\bar{\phi} - e_p$ plane has three types of structures: stable patterns; symmetric unstable patterns, and antisymmetric unstable patterns.

The upper curve in Figure 3 represents the boundary between the stable and unstable regions. We can see in this figure that there is a monotonic increase in the region of stability at increased values of e_p, as well as increased average solids-volume fraction, $\bar{\phi}$. Recall that the base-state transitions from a "Core-Annular" to a "Core-Segregation" structure when the value of e_p decreases from 1. From a physical standpoint, this contour map suggests gas-fluidized beds are more easily stabilized under densely packed conditions (that is, for $\bar{\phi} \approx \phi_{max}$), or when particle-particle collisions are highly elastic (that is, $e_p \approx 1$), such that the bed acquires a "Core-Annular" structure.

As shown in Figure 3, as $\bar{\phi}$ decreases in the unstable region, the dominant instability mode transitions from a symmetric to antisymmetric structure. In order to better understand the sensitivity of mode transition to particle packing, three ($\bar{\phi}$, e_p) points were selected in the unstable region of Figure 3: (0.1,0.96); (0.15,0.96); (0.2,0.96). The profiles of (dimensionless) growth rates (of the leading eigenvalues), and their corresponding (dimensionless) phase velocities are plotted in Figure 4. As illustrated in Figure 4a, growth rate, ξ, has two branches, which cross at a k_x value located at the point labeled **I**. At this point, there is a corresponding step change in the phase-velocity profile as shown in Figure 4b. The first branch labeled **S** in Figure 4a represents all symmetric mode structures, and the second branch labeled **A** represents all antisymmetric structures. Figure 4a shows that the maximum growth rates of both symmetric and antisymmetric branches increase with a decrease in the solids fraction. When $\bar{\phi}$ is equal to 0.2, the maximum growth rate of the dominant eigenvalue is 0.121 for the symmetric structure at $k_x = 0.5$, and the maximum growth rate of the antisymmetric branch is -0.017 at $k_x = 2.5$. Since the maximum growth rate of the second branch is negative, the system is stable to the antisymmetric disturbances. When $\bar{\phi}$ decreases to 0.15, the maximum growth rates of the symmetric and antisymmetric branches increase to 0.180 and 0.181 at $k_x = 0.65$ and 2.5, respectively, indicating that the growth of the antisymmetric perturbations is much faster than the symmetric perturbations with a decrease in $\bar{\phi}$. In this case, the system is equally unstable to the symmetric and antisymmetric disturbances. With a decrease in $\bar{\phi}$ to 0.1, the dominant mode transitions to the antisymmetric pattern, where the maximum growth rate of the dominant eigenvalue is 0.386 at $k_x = 2.5$. The profiles of the phase velocities corresponding to the leading eigenvalues are shown in Figure 4b. The phase velocity changes very slowly and smoothly with respect to k_x provided a mode transition is not observed in the corresponding eigenvalue profile. Note that as $\bar{\phi}$ decreases from 0.2 to 0.1, the phase velocity corresponding to the maximum growth rate in the symmetric branch increases from 10.72 to 11.60, while phase velocity (corresponding to maximum growth rate) for the antisymmetric branch increases from 9.57 to 9.92. Moreover, the magnitude of the phase velocities of the disturbances are slightly greater than the solid-phase velocities v^*, shown in velocity profiles (Figure 2d) at k_x values corresponding to maximum growth rates, but signifi-

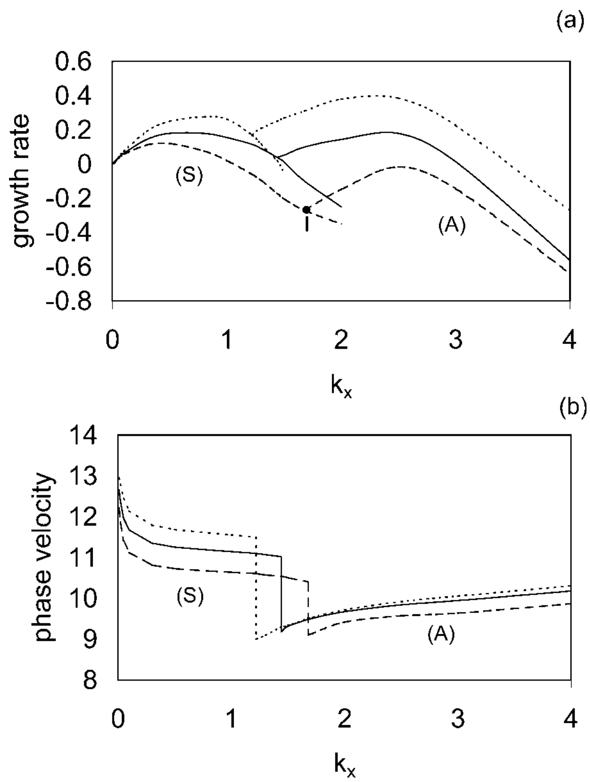

Figure 4. Variations of the growth rate of the leading mode and its phase velocity with k_x (e_p = 0.96, e_w = 0.6), ... $\bar{\phi}$ = 0.1, —— $\bar{\phi}$ = 0.15, ----- $\bar{\phi} = 0.2$.

(a) growth rate, and (b) phase velocity.

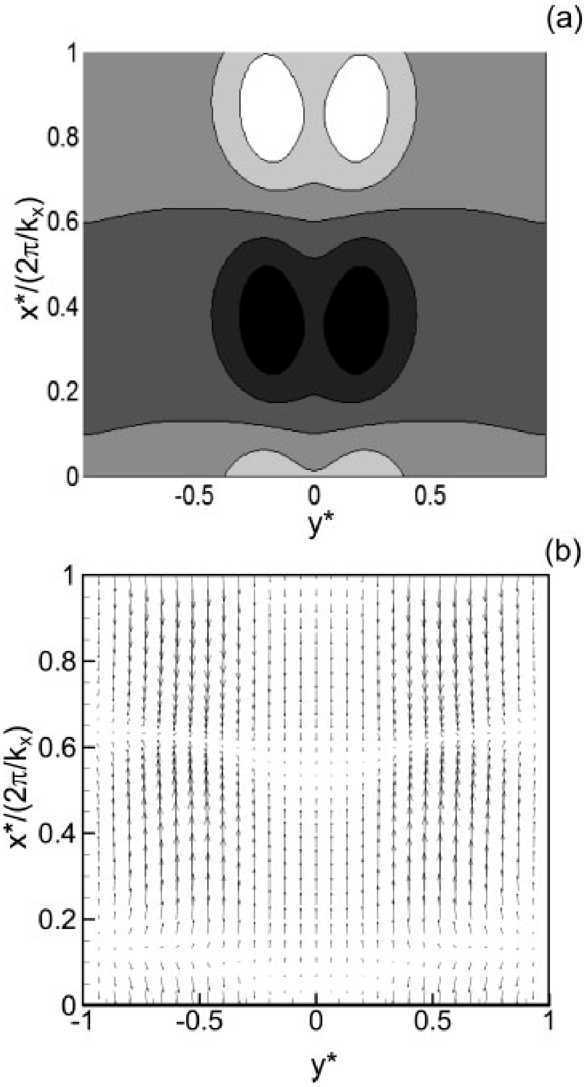

Figure 5. Eigenfunctions of the dominant mode with e_p = 0.96, $e_w = 0.6$ and $\bar{\phi} = 0.2$.

(a) Eigenfunctions associated with the solids fraction, and (b) Eigenfunctions associated with the solids-phase velocity. The eigenfunctions in this figure, and later figures are shown in a square box.

cantly less than gas-phase velocities, u^*, (shown in Figure 2c profiles). These results suggest that the propagation of the disturbance waves is primarily dominated by the solids phase. The similarity in magnitude of v^*, and the disturbance-phase velocity was also observed in granular flow. Wang et al.[36] reported that eigenmodes in granular flow within a channel are traveling waves, which move with a speed comparable to, but slightly greater than, that of the granular material itself.

The eigenfunctions corresponding to the dominant eigenvalues are plotted in Figures 5 and 6 for average solids-volume fractions $\bar{\phi} = 0.2$ and 0.1, respectively. Eigenfunctions associated with solids-volume fractions are plotted in Figures 5a and 6a, and eigenfunctions associated with solids-phase velocity are plotted in Figures 5b and 6b. In all figures, the eigenfunctions are plotted as spatial variations over one periodic cell of height $2\pi/k_x$. In both cases for $\bar{\phi}$, e_p and e_w are set at 0.96 and 0.6, respectively. For the denser of the two cases examined, ($\bar{\phi} = 0.2$), Figure 5a shows that the dominant mode has the form of symmetrical structures where particle-density patterns are symmetric about the centerline of the channel ($y^* = 0$). This means that traveling waves propagate upward through the column with alternating layers of dense and dilute regions. The eigenfunctions associated with the solid-phase velocity are shown in Figure 5b as a vector plot. It can be seen that over one periodic cell, the velocity profile vertically breaks down into two distinct regions corresponding to the distribution of the alternating density layers in Figure 5a. In particular, particle velocity has an upward fluctuation in dense layers and a downward fluctuation in dilute layers. Combining Figure 5a and b, we can

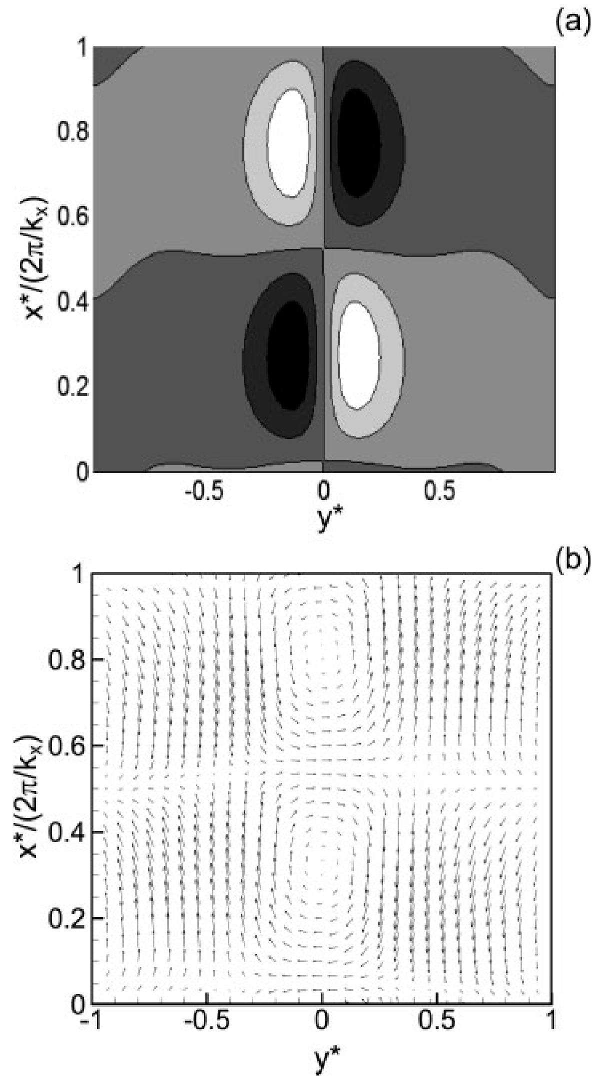

Figure 6. Eigenfunctions of the dominant mode with e_p = 0.96, e_w = 0.6 and $\bar{\phi}$ = 0.1.

(a) Eigenfunctions associated with solids fraction, and (b) Eigenfunctions associated with solids-phase velocity.

simply describe the motion of particles in gas-fluidized beds with a symmetrical perturbation in the following way: when the lower surface of the dense region becomes unstable, particles (within the solids-rich region) "rain" down to fill the dilute region below. Once they pass through the dilute region, they enter the upper surface of another solids rich region. Hence, for any particle-dense region, particles are lost from its lower surface and simultaneously collected on its upper surface. It is this mechanism that leads to the propagation of the density wave. A similar mechanism has been proposed by Glasser et al.[26] to explain the formation of bubbles and clusters in fluidized beds.

In the more dilute case ($\bar{\phi} = 0.1$), the dominant mode shown in Figure 6a has an antisymmetric structure with alternating regions of high and low-densities positioned on either side of the centerline. Although eigenfunctions associated with the solids-phase velocity vectors in the vertical direction (Figure 6b) appear similar to the symmetric case (where particles accelerate upward in dense regions and downward in dilute regions), lateral fluctuation becomes important in the antisymmetric structures, because the particle concentration has a significant gradient across the centerline. This is not the case for the symmetric structure as previously noted. As a result of the vertical and lateral components, recirculation loops are observed close to the centerline, where particles migrate from a dense (dilute) to a dilute (dense) region.

It is clear that there exist two types of disturbance structures in the gas-fluidized system, and that the leading instability mode can transition from one to the other at some value of k_x. However, whether or not this transition is smooth is still not known. To study the transition behavior, contour maps of the leading mode eigenfunctions (associated with solids fraction) are studied at several k_x points for a specific case corresponding to $\bar{\phi} = 0.15$ and $e_p = 0.96$. Under these conditions, the unstable mode was shown to transition at a value of the dimensionless vertical-wave number $k_x = 1.44$. For $k_x < 1.44$, the instability is dominated by a symmetric pattern, while the antisymmetric pattern dominates for $k_x > 1.44$. An examination of the eigenfunction plots just before and immediately following the transition point, shows a significant change in the nature of the instability structure. This suggests the transition is not smooth and indicates the two disturbance patterns develop independently with respect to k_x.

Another parameter we have considered in this work is the coefficient of particle-particle restitution e_p. In Figure 3, it was previously shown that all observed instabilities are driven by the inelastic nature of particle-particle collisions. In particular, the perfectly elastic system ($e_p = 1$) is always stable to small perturbations, and systems become less stable to small disturbances as e_p decreases from a value of one. It is interesting to note that for a range of $\bar{\phi}$ values from 0.10 to 0.15, the unstable modes have two transition points with a decrease in e_p; the first represents a transition from a symmetric to antisymmetric structure; and the second represents a reverse transition back to a symmetric pattern (see Figure 3). To further investigate the origin of these two transition points, growth rates and phase velocities of the disturbance are plotted as a function of wave number, k_x for solids-volume fraction $\bar{\phi} = 0.15$ at various values of e_p in Figure 7. In Figure 7a, as e_p decreases from 0.98 to 0.965, the instabilities in both branches are significantly enhanced, and the leading eigenvalue in the antisymmetric branch becomes larger than that in the symmetric branch. Hence, there exists a transition from a symmetric to antisymmetric pattern under these conditions. However, as e_p decreases beyond this point, that is, from 0.965 to 0.95, the potential exists for the dominant instability mode to transition back to the symmetric pattern since, within this range of e_p values, the growth of the leading eigenvalue in the symmetric branch becomes larger than that of the antisymmetric branch. A comparison of Figures 4 and 7 shows that with decreasing $\bar{\phi}$, the k_x point corresponding to the transition of the two leading eigenvalue branches shifts to the left allowing the antisymmetric branch to become dominant within a larger range of k_x values. Conversely, as e_p decreases, the range of k_x values at which the antisymmetric branch dominates is restricted.

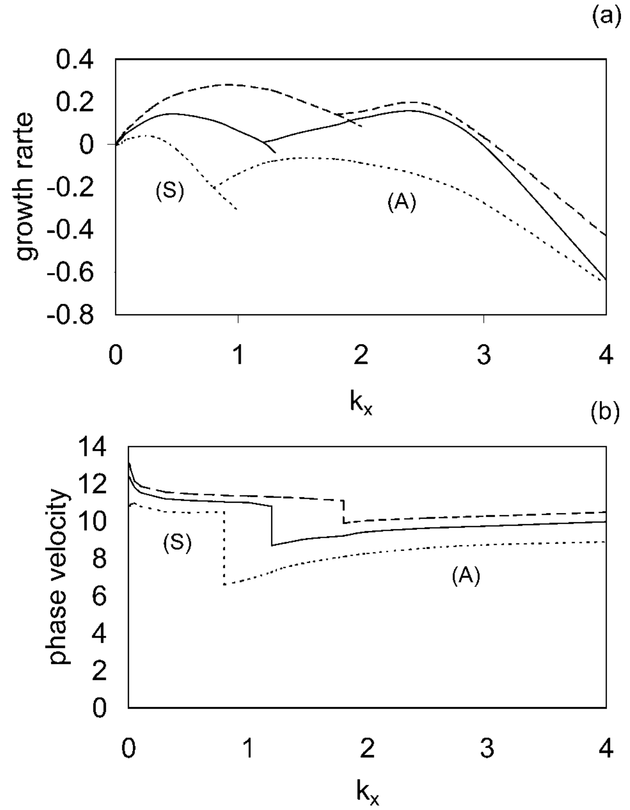

Figure 7. Variations of the growth rate of the leading mode and its phase velocity with k_x for different coefficients of restitution e_w = 0.6, $\bar{\phi}$ = 0.15, ... e_p = 0.98, —— e_p = 0.965, ----- e_p = 0.96.

(a) Growth rate, and (b) phase velocity.

We now consider a stability analysis for the source-wall condition when e_w increases to values of 0.98. To compare these results to those for the sink-wall condition (see Figures 4–6), two cases have been selected, ($\bar{\phi} = 0.1$, $e_p = 0.96$, $e_w = 0.98$) and ($\bar{\phi} = 0.2$, $e_p = 0.96$, $e_w = 0.98$). Figure 8 shows that for the source wall case, the growth-rate profiles still have two branches; the first branch represents the symmetric pattern, and the second one represents the

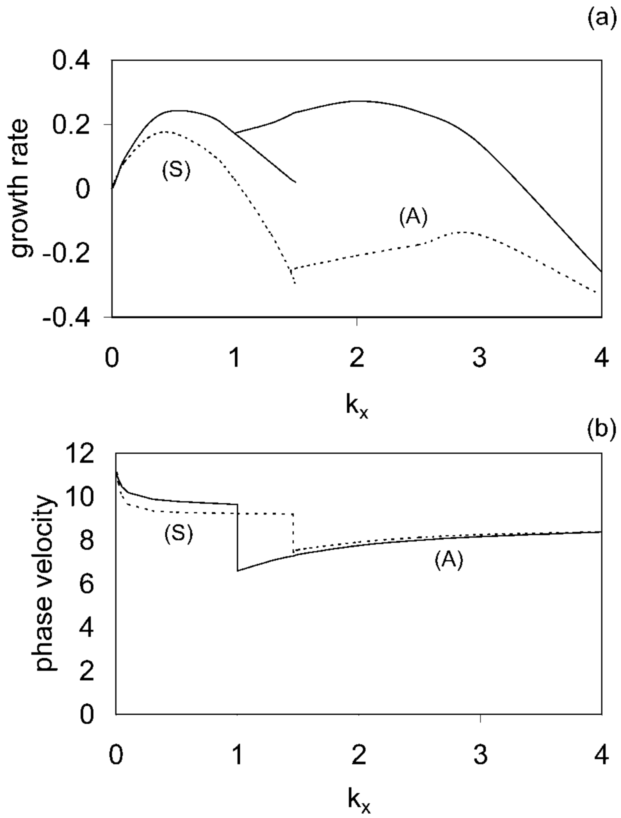

Figure 8. Variations of the growth rate of the leading mode, and its phase velocity with k_x under the source-wall condition, e_p = 0.96, e_w = 0.98, —— $\bar{\phi}$ = 0.1, ... $\bar{\phi}$ = 0.2.

(a) Growth rate, and (b) phase velocity.

antisymmetric pattern. It is important to note that the instability patterns under the source-wall conditions are very similar to those under the sink wall conditions. In fact, there are only slight differences in the wave number values of the transition point, and the maximum growth rates of the two branches. Similarities in stability behavior in the two wall conditions suggest insensitivity to e_w. This can also be observed in the eigenfunction contour plots. When we examine the solids-fraction eigenfunctions corresponding to the dominant eigenvalues under conditions of ($\bar{\phi} = 0.1$, $e_p = 0.96$, $e_w = 0.98$) and ($\bar{\phi} = 0.2$, $e_p = 0.96$, $e_w = 0.98$) (not shown), we find that the contour maps of the eigenfunctions associated with the solids fractions are almost indistinguishable between the sink-wall and source-wall cases (respectively).

We believe the observed insensitivity of stability behavior to e_w is due to the similarity of the solids-fraction profiles of the base states (Figures 1a and 2a). In particular, for values of $e_p < 0.99$, particles are always segregated in the center, and the contribution of e_w on particle profile is small. For values of $e_p > 0.99$, the difference between the solids-fraction profiles in the sink-wall and source-wall conditions becomes pronounced. However, in this case, the dominant eigenvalue becomes negative (see Figure 3), and the gas-fluidized bed system is stable to small perturbations.

The effect of another wall parameter, the specularity coefficient, is also investigated. We find both steady-state solutions and instability modes are not sensitive to this parameter. Since we have already shown that the instability behavior is not sensitive to the particle-wall restitution coefficient, we can conclude that the instability behavior in the gas-fluidized bed we considered is not sensitive to the nature of boundaries. Similar results have been obtained in granular channel flows. Wang and Tong[37] compared the instability features of granular channel flows for adiabatic wall conditions and sink-wall conditions. They found the instabilities were not sensitive to the boundary conditions.

Finally, the steady-state solution is augmented with a small perturbation to examine its spatiotemporal effect according to $\phi_t = \hat{\phi}_1 \exp(st*) \exp(k_x x*) + \phi_0$, where ϕ_0 is the base-state solids fraction, and ϕ_t is the time-dependent solids fraction. Figure 9 shows the results for a system dominated by the antisymmetric perturbations. From time equal to zero, a streamer-like solution forms in the center due to the instability patterns (see the eigenfunction plot in Figure 9), and moves upward in a "snake-like" fashion, oscillating to a greater extent about the center with time. When the dominant eigenfunctions are symmetric, the evolution of the instability behavior is markedly different (see Figure 10). Since particles are initially segregated at the center in the base-state condition and dominant instabilities are also observed at the center (see the eigenfunction plot in Figure 10), a cluster-like structure can be captured immediately. In addition, with increasing time the low-density regions (located near the walls in the base state) migrate to the center and coalesce to form a compact region of low-density. At this point, alternating regions of low and high-density can be seen moving throughout the bed. Finally, the pattern develops in a bubble-like structure. More time is required to capture the formation and propagation of bubble-like structures due to the solids distribution of the base state.

From Figures 9 and 10, it can be seen that there is little to no change in density structure in regions near the wall, and that most of the changes are observed at the center. Therefore, it is clear that the boundaries serve to stabilize the system, and that instability structures develop in the center region. In addition, the results in Figure 3 together with those in Figures 9 and 10 provide a possibility to qualitatively compare the simulation results with experimental measurements. Experimental measurements have shown that bubbling patterns develop in dense-fluidized beds,[1] and streamer-like patterns develop in dilute systems.[1,3] Figure 3 indeed predicts that bubble-like structures should develop in relatively dense-fluidized beds, while streamer-like structures should develop in relatively dilute systems. If experiments are designed for measuring the variation of the instability structures with the variation of the mean-solids fraction (0.05–0.5), quantitative comparison between simulation results and experimental work becomes possible.

The physical mechanism of instability formation and propagation discussed in the previous section is examined by analyzing the governing equations term-by-term. It is well known that the instability of fluidized beds is of an inertial nature.[14,15] Hirayama and Takaki[15] reported that for an unbounded liquid-fluidized bed, the fluid inertial term is responsible for the instability. In gas-particle beds, however,

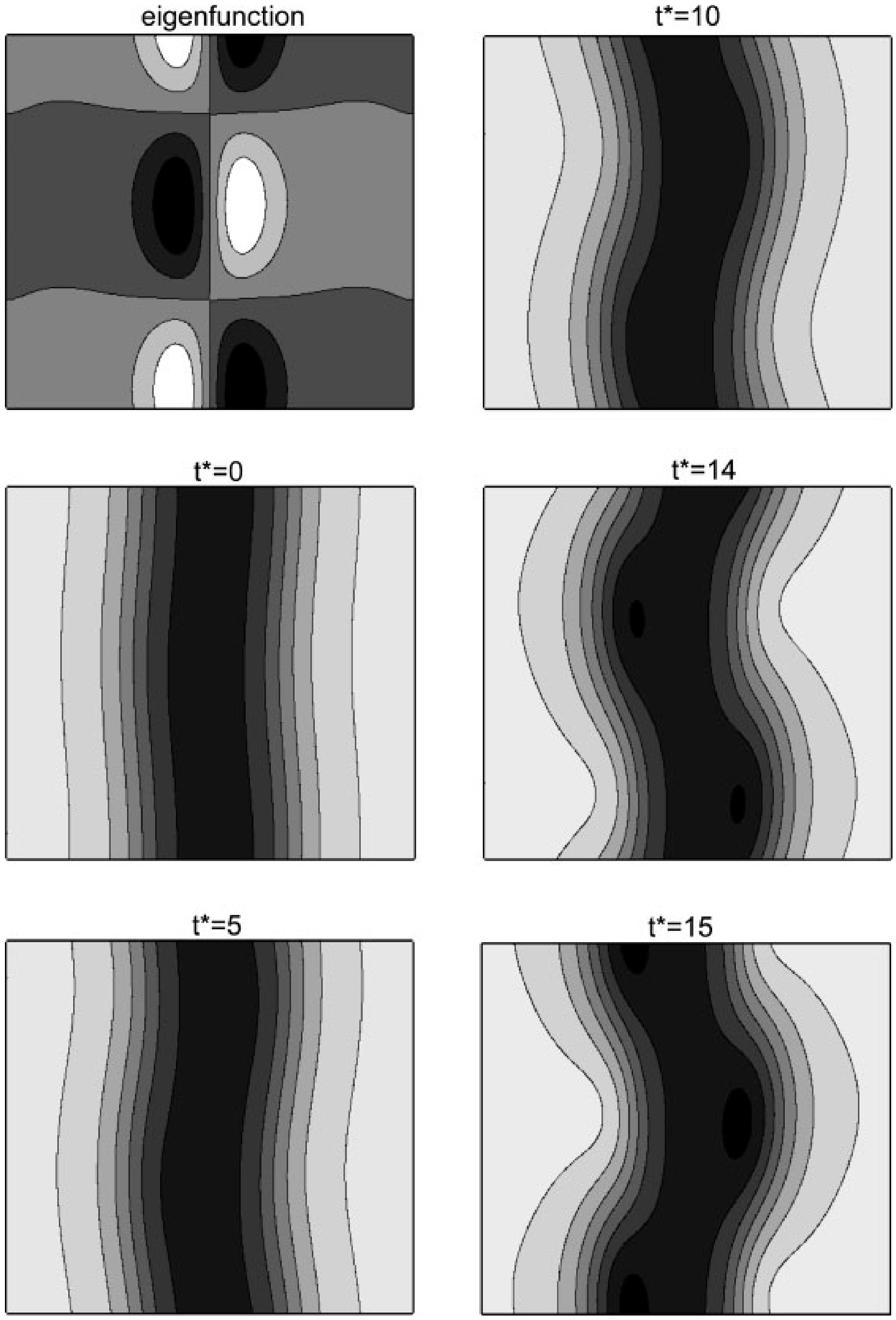

Figure 9. Temporal evolution of the density waves with the antisymmetric dominant instability patterns where the scale for the evolution contour plots is from 0 (white) to 0.65 (black).

$e_p = 0.96$, $e_w = 0.6$, $\bar{\phi} = 0.15$, $k_x = 2.5$.

fluid-phase inertia is very small (and often neglected). Hence, its inertial contribution to instability formation should be much smaller than in liquid-fluidized beds, while the contribution of solids phase inertia should be more pronounced.

For a system dominated by the antisymmetric instability mode ($\bar{\phi} = 0.1$, $e_p = 0.96$, $e_w = 0.6$), the dominant instability pattern first transitions to symmetric structures, and then the dominant eigenvalue decreases to a negative value when the contribution of solids inertial terms decreases. With a decrease in the gas inertial terms, the dominant instability pattern remains antisymmetric, and the dominant eigenvalue remains positive.[43] Calculations have also been carried out for the case when the system instability is dominated by symmetric patterns (that is, $\bar{\phi} = 0.2$, $e_p = 0.96$, $e_w = 0.6$). We find that the dominant instability pattern transitions to antisymmetric structures when the gas inertial terms are not considered, while a transition from the symmetric instability pattern to a stable pattern is observed when the solids inertial terms are removed. Therefore, the solids inertia plays a critical role in the instability. Without

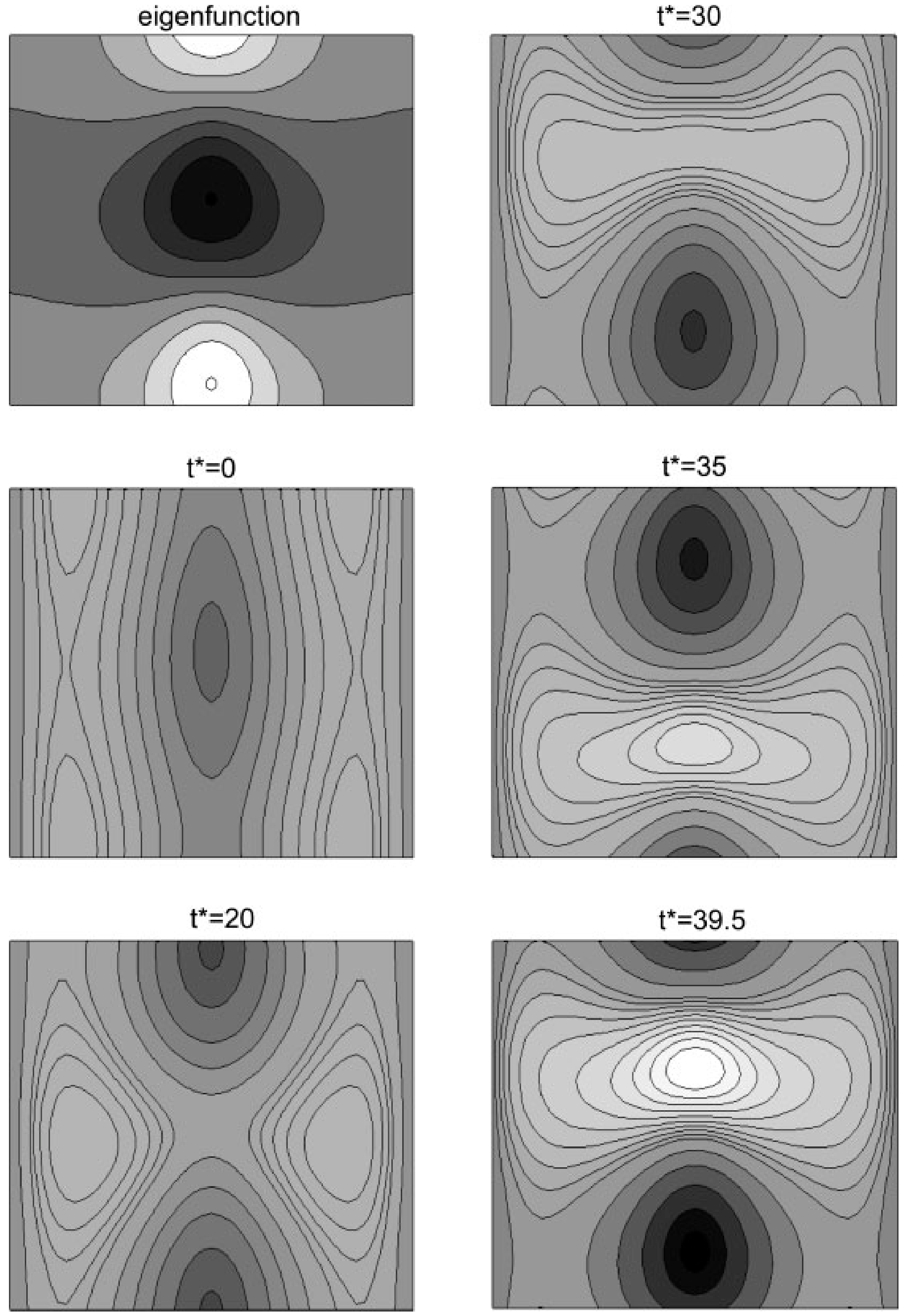

Figure 10. Temporal evolution of the density waves with the symmetric dominant instability patterns where the scale for the evolution contour plots is from 0 (white) to 0.35 (black).

$e_p = 0.985$, $e_w = 0.6$, $\bar{\phi} = 0.1$, $k_x = 0.3$.

this term, gas-fluidized beds are always stable to small perturbations. Similar results were also obtained from the work of Wang and Tong.[37] They found in a granular channel flow driven by gravity that the dominant eigenvalue monotonically decreases with a decrease in the solid-phase inertial term. The contribution of the gas inertial terms on the origin of the instability is less important. The fluidized-bed system may still lose stability to small disturbances when this term is absent. When the system becomes unstable the solids inertia and gas inertia have different effects on the development of instabilities. The development of the symmetric patterns is mainly due to the contribution of the gas inertial terms, while the development of the antisymmetric patterns is mainly due to the contribution of the solid-phase inertial terms.[43] Without the gas inertia term, only antisymmetric structures can be observed, based on our linear stability analysis.

We have shown that the inertial terms have a significant effect on the instability patterns. However, it is not clear why the gas-phase inertia is significant. Therefore, a further investigation of the inertial force profiles across the bed is carried out. We define the following terms

$$gas\_x = DE(1-\phi^0)\left(s\hat{u}_x + ik_x u_x^0 \hat{u}_x + \hat{u}_y \frac{du_x^0}{dy^*}\right) \tag{8}$$

$$gas\_y = DE(1-\phi^0)(s\hat{u}_y + ik_x u_x^0 \hat{u}_y) \tag{9}$$

$$solids\_x = D\phi^0\left(s\hat{v}_x + ik_x v_x^0 \hat{v}_x + \hat{v}_y \frac{dv_x^0}{dy^*}\right) \tag{10}$$

$$solids\_y = D\phi^0(s\hat{v}_y + ik_x v_x^0 \hat{v}_y) \tag{11}$$

Here, Eqs. 8 and 9 represent the dimensionless gas phase inertial forces in the vertical *(x)* and lateral *(y)* directions, respectively, and Eqs. 10 and 11 represent the dimensionless solids-phase inertial forces in the x and y directions, respectively. When the instability is dominated by the symmetric patterns (see Figure 5a), the inertial forces in x are symmetric between the centerline, while the profiles of the inertial forces in y are antisymmetric (see Figure 11a). In addition, the inertial forces in x are much larger than in y. Thus, the velocity fluctuation is mainly in the vertical direction (see Figure 5b). In the vertical direction, although the absolute value of the solids-phase inertial force is larger than the gas phase, their absolute values have the same order of magnitude across the bed, except in the region near the center. This can be attributed to the gas velocity and the solids-volume fraction profiles in the base state, since a significant increase in gas velocity is observed close to the walls where the solids fraction is low (see Figure 2). Hence, the gas-phase inertial force has a pronounced effect on the symmetric instabilities. When the instability is dominated by the antisymmetric patterns (see Figure 6a), the inertial forces in the vertical direction are antisymmetric, while the profiles of the inertial forces in the lateral direction are symmetric. Moreover, the inertial forces of the gas phase are much smaller than the solid phase. Thus, the antisymmetric instability is dominated by the solids-phase inertial force. In addition, the values of the solid-phase inertial force has the same order of magnitude in both the x and y direction. Therefore, the lateral fluctuation in velocity profile becomes important, and recirculation loops can be observed in the center (see Figure 6b).

The effect of the "energy inertia" term $\frac{\partial(\frac{3}{2}\rho_s\phi T)}{\partial t} + \nabla\cdot(\frac{3}{2}\rho_s\phi T\underline{v})$, on the instability modes is also examined. We find that the value of the dominant eigenvalue increases with a decrease in the contribution of this term. Thus, the "energy inertia" serves to stabilize the system. Similar results have been found in granular channel flows.[37]

The effect of e_p on the nature of the instability has previously been discussed. Since the constitutive relationships used in this model are based largely on the use of slightly inelastic particles, the contribution of e_p will primarily affect the dissipation term (J_{coll}) in the pseudo-thermal energy-balance equation. We find the sensitivity of the steady-state flow structures to e_p is due to a rapid increase in the dissipation term as the system transitions from an elastic to slightly inelastic case. If the contribution of J_{coll} is reduced, the sensitivity can be suppressed. When J_{coll} is eliminated, a "Core-Annular" structure is observed for steady-state flows. This topic has been discussed in a number of articles.[32–35,51–53] For both symmetric ($\bar{\phi} = 0.2$, $e_p = 0.96$ and $e_w = 0.6$) and anti-symmetric ($\bar{\phi} = 0.1$, $e_p = 0.96$ and $e_w = 0.6$) dominant instabilities, the maximum growth rates decrease rapidly with a decrease in the contribution of the dissipation term.[43] We find in the energy-balance equation, if the energy dissipation term has a relatively small value the system can remain stable to small perturbation. The reason that energy dissipation can initiate instabilities is because granular materials can spontaneously generate clusters due to inelastic collisions.[54] Assuming the particle concentration has a small increase in a region due to a flucturation, the granular temperature will decrease in this region than in the neighboring regions, because the frequency of inelastic collisions is larger in this region relative to neighboring, less dense region, leading to more energy loss in the dense region. This leads the particle pressure to form a gradient from the less dense region to this dense region, causing a migration of more particles into this region, thus, further increasing its density and decreasing its pressure. Thus, a dense cluster can form. When this dissipation term is removed, the system is always stable to small perturbations. Therefore, we can conclude that for the system to lose stability one must include both the solid-phase inertial and the granular energy-dissipation terms, otherwise the system is stable to small perturbations.

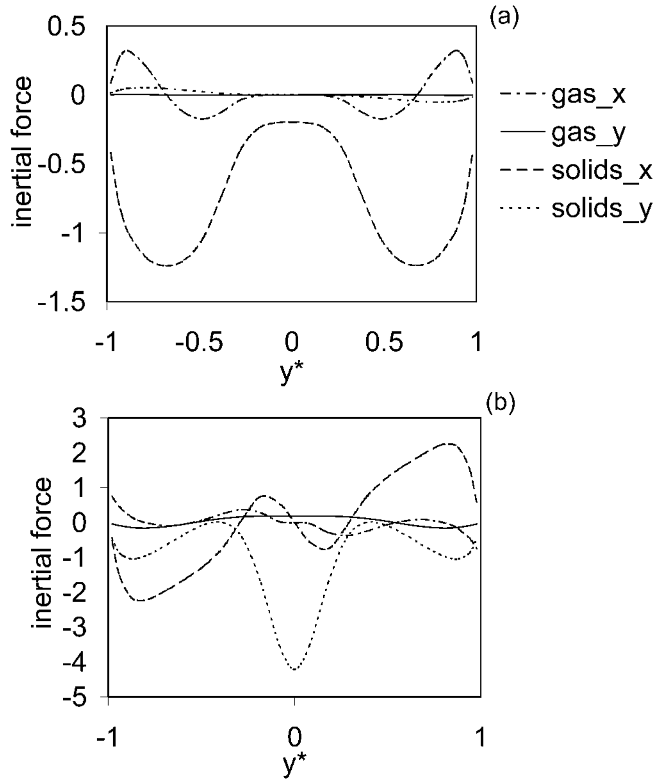

Figure 11. Inertial force profiles, e_p = 0.96, e_w = 0.6. (a) symmetric instability patterns ($\bar{\phi}$ = 0.2), and (b) antisymmetric instability patterns ($\bar{\phi}$ = 0.1).

Conclusions

In this article, a continuum approach has been used to examine the hydrodynamic stability behavior of gas-fluidized beds, having bounded walls, using constitutive relationships adopted from the kinetic theory of granular flow. Steady-state, fully developed flows are first obtained using a numerical method, based on an orthogonal collocation algorithm. The nature of predicted instabilities of the steady-state solution are, subsequently, examined using classical methods of linear stability theory.

For all the cases we have studied we observe that the dominant instability has either the form of a symmetric or antisymmetric traveling wave. An increase in solids-volume fraction, and a decrease in particle-particle inelasticity were both shown to suppress the wavy disturbance. With variations in the solids fraction and the coefficient of particle-particle restitution, transitions between the two observed instability modes were observed. In this work, we find that computed eigenmodes are in the form of traveling waves, which move at a speed comparable to the velocity of the solid phase. Instability behavior in the source and sink-wall conditions are compared. Results show that, for both wall conditions, the leading eigenvalue profiles and dominant eigenfunction contour maps are insensitive to the physical nature of the boundary walls. This is presumably due to the similarity of the base state solids-volume fraction profiles. While we have examined a number of different combinations of parameters and found that the dominant instability pattern is a symmetric or antisymmetric traveling wave, we cannot rule out qualitatively different behavior for parameter combinations not considered in this work.

The physical mechanism of unstable waveforms was investigated using a term-by-term method of analysis. We found both the gas and solid-phase inertial terms to be primarily responsible for instability formation in gas-fluidized beds. In particular, if the solid-phase inertial term is sufficiently small, all eigenmodes are stable. The gas and solid-phase inertial terms were shown to have markedly different effects on the structure of the instability, that is, the development of the symmetric pattern is due to the contribution of the gas-phase inertial terms, while the development of the antisymmetric patterns is due to the contribution of the solid-phase inertial term. The inelasticity of particle-particle collisions can also significantly impact the origin of instabilities in gas-fluidized beds by affecting the contribution of the dissipation term in the pseudo-thermal energy balance (Eq. 5). Specifically, decreasing particle-particle inelasticity is known to reduce energy fluctuation dissipation, and this results in a rapid suppression of the instability.

One of the main assumptions in linear-stability theory is that short temporal evolution can be governed by linear instabilities. It is this assumption that forms the basis of results presented in Figures 9 and 10. More importantly, we need to determine how these waves grow over longer duration (when nonlinear terms dictate behavior), and whether or not the patterns that develop resemble those predicted by linear theory. These questions can be answered by a transient integration approach. Hence, it is of interest to extend the transient work to gas-fluidized systems to examine how density waves predicted in this analysis, will develop temporally using nonlinear theory.

Acknowledgments

This work has been partially supported by the National Aeronautics and Space Administration, American Chemical Society Petroleum Research Fund and National Science Foundation.

Literature Cited

1. Kunii D, Levenspiel O. Fluidization Engineering. Butterworth-Heinemann; 1991.
2. Helland E, Occelli R, Tadrist L. Numerical study of cluster formation in a gas-particle circulating fluidized bed. *Powder Technol.* 2000;110:210–21.
3. Juan AH. Instabilities induced by concentration gradients in dusty gases. *J Fluid Mech.* 2001;435:247–60.
4. Agrawal K, Loezos P, Syamlal M, Sundaresan S. The role of meso-scale structures in rapid gas-solid flows. *J Fluid Mech.* 2001;445:151–85.
5. Jackson R. *The Dynamics of Fluidized Particles.* Cambridge University Press; 2000.
6. Lun CKK, Savage SB, Jeffrey DJ, Chepurniy N. Kinetic theories for granular flow: inelastic particles in couette flow and slightly inelastic particles in a general flow field. *J Fluid Mech.* 1984;140:223–56.
7. Lun CKK. Kinetic theory for granular flow of dense, slightly inelastic, slightly rough spheres. *J Fluid Mech.* 1991;233:539–59.
8. Jenkins JT, Savage SB. A theory for the rapid flow of identical, smooth, nearly elastic, spherical particles. *J Fluid Mech.* 1983;130:187–202.
9. Jenkins JT, Richman M. Kinetic theory for plane flows of a dense gas of identical, rough, inelastic, circular disks. *Phys Fluids.* 1985;28:3485–94.
10. Anderson TB, Jackson R. A fluid mechanical description of fluidized beds. Equations of motion. *Ind Eng Chem Fundam.* 1967;6:527–39.
11. Anderson TB, Jackson R. Fluid mechanical description of fluidized beds. Stability of the state of uniform fluidization. *Ind Eng Chem Fundam.* 1968;7:12–21.
12. Pigford RL, Baron T. Hydrodynamic stability of a fluidized bed. *Ind Eng Chem Fundam.* 1965;4:81–7.
13. Bachelor GK, Nitsche JM. Instability of stationary unbounded stratified fluid. *J. Fluid Mech.* 1991;227:357–91.
14. Jackson R. The mechanics of fluidized beds. I: the stability of the state of uniform fluidization. *Trans. Inst Chem Eng.* 1963;41:13–21.
15. Hirayama O, Tsuzuki T. Linear stability of a two-dimensional uniform fluidized beds. *Fluid Dyn Res.* 1995;15:425–35.
16. Bachelor GK. Secondary instability of a gas-fluidized bed. *J Fluid Mech.* 1993;257:359–71.
17. Koch DL, Sangani AS. Particle pressure and marginal stability limits for a homogeneous monodisperse gas fluidized bed: kinetic theory and numerical simulation. *J Fluid Mech.* 1999;400:229–63.
18. Fanucci JB, Ness N, Yen RH. On the formation of bubbles in gas-particle fluidized beds. *J Fluid Mech.* 1979;94:353–67.
19. Hirayama O, Takaki R. Analysis of nonlinear waves in a one-dimensional fluidized bed. *Fluid Dyn Res.* 1997;21:233–47.
20. Liu JTC. Nonlinear unstable wave disturbances in fluidized beds. *Proc. R. Soc Lond A.* 1983;389:331.
21. Needham DJ, Merkin JH. The propagation of voidage disturbances in a uniform fluidized bed. *J Fluid Mech.* 1983;131:427–54.
22. Glasser BJ, Kevrekidis IG, Sundaresan S. One- and two-dimensional traveling wave solutions in gas fluidized beds. *J Fluid Mech.* 1996;306:183–221.
23. Goz MF. On the origin of wave patterns in fluidized beds. *J Fluid Mech.* 1992;240:379–404.
24. Goz MF. Bifurcation of plane voidage waves in fluidized beds. *Physica D.* 1993;65:319–51.
25. Glasser BJ, Kevrekidis IG, Sundaresan S. Fully developed traveling wave solutions and bubble formation in fluidized beds. *J Fluid Mech.* 1997;334:157–88.

26. Glasser BJ, Sundaresan S, Kevrekidism IG. From bubbles to clusters in fluidized beds. *Phys Rev Lett*. 1998;81:1849–52.
27. Anderson TB, Jackson R. Fluid mechanical description of fluidized beds. Comparison of theory and experiment. *Ind Eng Chem Fundam*. 1969;8:137–44.
28. El-Kaissy MM, Homsy GM. Instability waves and the origin of bubbles in fluidized beds. I: Experiments. *Int J of Multiphase Flow*. 1976;2:379–395.
29. Bader R, Findlay J, Knowlton T. Circulating Fluidized Bed Technology II. Pergamon, New York; 1988.
30. Yerushalmi J, Cankurt N, Geldart D, Liss B. Flow regimes in vertical gas-solid contact system. *AIChE Symp Ser*. 1978;74:1–13.
31. Nieuwland JJ, van Sint Annaland M, Kuipers JAM, van Swaaij WPM. Hydrodynamic modeling of gas/particle flows in riser reactors. *AIChE J*. 1996;42:1569–82.
32. Pita JA, Sundaresan S. Gas-solid flow in vertical tubes. *AIChE J*. 1991;37:1009–18.
33. Sinclair JL, Jackson R. Gas-particle flow in a vertical pipe with particle-particle interactions. *AIChE J*. 1989;35:1473–86.
34. Ocone R, Sundaresan S, Jackson R. Gas-particle flow in a duct of arbitrary inclination with particle-particle interactions. *AIChE J*. 1993;39:1261–71.
35. Liu X, Glasser BJ. A parametric investigation of gas-particle flow in a vertical duct. *AICHE J*. 2006;52:940–56.
36. Wang CH, Jackson R, Sundaresan S. Instabilities of fully developed rapid flow of a granular material in a channel. *J Fluid Mech*. 1997;342:179–97.
37. Wang CH, Tong Z. On the density waves developed in gravity channel flows of granular materials. *J Fluid Mech*. 2001;435:217–46.
38. Hui K, Haff PK, Ungar JE, Jackson R. Boundary conditions for high-shear grain flows. *J Fluid Mech*. 1984;145:223–33.
39. Jenkins JT, Richman MW. Boundary conditions for plane flows of smooth, nearly elastic, circular disks. *J Fluid Mech*. 1986;171:53–69.
40. Johnson PC, Jackson R. Frictional-collisional constitutive relations for granular materials, with application to plane shearing. *J Fluid Mech*. 1987;176:67–93.
41. Richman MW. Boundary conditions based upon a modified Maxwellian velocity distribution for flows of identical, smooth, nearly elastic spheres. *Acta Mehcanica*. 1988;75:227–40.
42. Constantinides A. *Chemical Engineering Series-Applied Numerical Methods with Personal Computers*. McGraw-Hill, Inc; 1987.
43. Liu X. Instability and *Segregation in Bounded Gas-Particle Fluidized Beds and Granular Flows*. Rutgers Univeristy, New Bruniswick; 2006. Ph.D. Thesis.
44. Wang CH. *Instabilities in granular material flows*. Princeton University, 1995. Ph.D. Thesis.
45. Wang CH, Jackson R, Sundaresan S. Stability of bounded rapid shear flows of a granular material. *J Fluid Mech*. 1996;308:31–62.
46. Cody GD, Goldfarb DJ, Storch GVJ, Norris AN. Particle granular temperature in gas fluidized beds. *Powder Technol*. 1996;87:211–32.
47. Poilashenski W, Chen JJC. Normal solid stress in fluidized beds. *Powder Technol*. 1997;90:13–23.
48. Miller A, Gidaspow D. Dense, vertical gas-solid flow in a pipe. *AIChE J*. 1992;38:1801–15.
49. Mathiesen V, Solberg T, Hjertager BH. An experimental and computational study of multiphase flow behavior in a circulating fluidized bed. *Int J of Multiphase Flow*. 2000;26:387–419.
50. Benyahia A, Arastoopour H, Knowlton TM, Massah H. Simulation of particles and gas flow behavior in the riser section of a circulating fluidized bed using the kinetic theory approach for the particulate phase. *Powder Technol*. 2000;112:24–33.
51. Louge MY, Mastorakos E, Jenkins JT. The role of particle collisions in pneumatic transport. *J Fluid Mech*. 1991;231:345–59
52. Hrenya CM, Sinclair JL. Effects of particle-phase turbulence in gas-solid flows. *AIChE J*. 1997;43:853–69.
53. Eduardo JB, Yasuna JA, Sinclair JL. Dilute turbulent gas-solid flow in risers with particle-particle interactions. *AIChE J*. 1995;41:1375–88.
54. Goldhirsch I. Rapid granular flows. *Ann Rev Fluid Mech*. 2003;35:267–93.

Manuscript received Jun. 1, 2006, and revision received Dec. 23, 2006.